NASA Contractor Report 180830

Fraction Eutectic Measurements in Slowly Cooled Pb—15 wt % Sn Alloys

Anthony C. Studer and V. Laxmanan

Case Western Reserve University
Cleveland, Ohio

June 1988

Prepared for
Lewis Research Center
Under Grant NCC 3-74

National Aeronautics and
Space Administration

FRACTION EUTECTIC MEASUREMENTS IN SLOWLY COOLED Pb - 15 wt % Sn ALLOYS

Anthony C. Studer and V. Laxmanan

Department of Material Science and Engineering
Case Western Reserve University
Cleveland, Ohio 44106

Abstract

A space shuttle experiment employing the General Purpose Furnace (GPF) in its isothermal mode of operation is currently manifested for flight circa 1989. The central aim of this experiment is to investigate the role of gravity in a slowly, and isothermally, cooled sample (cooling rates about 0.003 K/sec, thermal gradients <0.05 K/mm, the top slightly hotter than the bottom) of a binary Pb - 15 wt % Sn alloy. Ground-based work in support of the microgravity experiment will be discussed. In particular, it will be shown that fraction eutectic measurements using an image analyzer, can be used to satisfactorily describe macrosegregation occurring in these slowly cooled ingots.

Introduction

In most solidification processes, there is usually insufficient time for complete diffusional equilibrium to be established within both the solid and liquid phases. This leads to concentration gradients within the liquid and the solid, and a solute buildup ahead of the solid-liquid interface. Hence, even in a nominally single phase alloy (1,2), such as lead - 15 wt % tin alloy, a two phase eutectic solid is formed when the liquid composition reaches the eutectic composition. The amount of eutectic formed is also affected by fluid flow during solidification. In this investigation, which was aimed at understanding the segregation occurring in slowly cooled lead - tin alloys, the spatial variation of fraction eutectic in the sample was proposed as a suitable means for determining the extent of macrosegregation.

The compositional variation within the solidifying dendrite may be described by the "local" solute redistribution equation derived by Bower, Brody and Flemings (3), assuming unidirectional growth, no fluid flow effects and negligible diffusion in the solid during freezing:

$$C_s^* = C_o[s + k(1 - s)f_L^{k-1}] \tag{1}$$

where

$$s = ak/(k - 1) = D_L G_L/R\ \Delta T_o \tag{2}$$

Thus, in the ideal case of unidirectional, (essentially) isothermal, dendritic, solidification (that is when G_L/R is very small) the Chalmers number, s, defined by Equation (2) (4) is very nearly zero and Equation (1) reduces to the classical nonequilibrium solidification equation (5-7):

$$C_s^* = kC_o(1 - f_s)^{k-1} \tag{3}$$

It is important to note that in deriving Equation (1) the differential volume element considered is of the scale of the dendrite arm spacing, but in deriving Equation (3) the volume element is usually taken to be the entire ingot. Thus, Equation (3) describes "local" compositional variations (microsegregation) within a dendritically grown ingot, as well as the macroscale variation of composition (macrosegregation) across an entire ingot solidified with a planar interface (8). Solids grown with a planar interface, such as doped silicon ingots for semiconductor applications, are usually grown with a positive temperature gradient ($s > 1$).

Let C_s denote the average composition of the dendrite and the two-phase solid formed within a small volume element and $f_{\alpha\beta}$ the amount of two-phase, "eutectic-like," solid formed during two-phase ("eutectic") solidification.

$$\overline{C}_s = \overline{C}_\alpha f_\alpha + \overline{C}_{\alpha\beta} f_{\alpha\beta} \tag{4}$$

where

$$\overline{C}_\alpha = \int_o^{f_\alpha} C_s^* \, df_s \Big/ \int_o^{f_\alpha} df_s \tag{5}$$

$$f = [(kC_E - sC_o)/kC_o(1 - s)]^{1/(k-1)} \tag{6}$$

and

$$\overline{C}_{a\beta} = C_E - s\,\Delta C_o \tag{7}$$

Equation (6) is obtained from Equation (1) by setting $C_s^* = kC_E$ corresponding to $f_L = f_{\alpha\beta}$. Equation (7) follows from a solute balance at the eutectic front (1,2). Assumptions used to derive Equations (1) to (7), in addition to the two already mentioned, are: (1) the partition ratio, k, is a constant; (2) the solid-liquid interface is at "local" thermodynamic equilibrium; (3) surface tension effects are negligibly small; and (4) no undercooling prior to eutectic or two-phase solidification.

Note that the composition of the two-phase solid forming within the interdendritic regions is less than the eutectic composition if solidification occurs in a positive temperature gradient (9). The two-phase solid, however, still looks like a eutectic. The amount of two-phase solid formed, as given by Equation (6), is also less than the amount that would be obtained from the Scheil equation (Equation (3) above) when s is positive. For $s = 0$, equation (6) gives the Scheil eutectic value.

Although the term "eutectic" will be used here, we are referring in general to a two-phase solid whose composition may or may not be equal to eutectic composition.

Also, it may be readily shown that the average composition of a completely solidified element obtained by using Equations (1) and (5) to (7) in Equation (4), or using Equations (3) and (5) in Equation (4), is exactly equal to C_o. This means that if solute redistribution is described by either Equations (1) or (3), there will be no macroscale segregation in the solidified ingot. Compositional variations observed will be strictly on the microscopic scale of the dendrite arm spacing (10). This also means that there is no single unique value of fraction eutectic (or fraction two-phase solid), f_E (or $f_{\alpha\beta}$) that may be associated with lack of macrosegregation. The value of f_E or $f_{\alpha\beta}$ corresponding to no macrosegregation depends on the growth conditions and also on the detailed assumptions used in the model for solute redistribution, Figure 1.

In general if there is macrosegregation in the ingot, C_s will be greater than, less than, or equal to the initial alloy composition, C_o at various locations in the sample. This is usually explained by assuming that solute flow must have occurred between volume elements (11-14). If there is a net flow of solute out of an element, that element would have a lower fraction of eutectic. And for the opposite situation, where the net flow of solute is into the element, the amount of eutectic present would increase. Hence, by measuring the variation in the amount of eutectic phase one can describe the macrosegregation within an ingot.

The assumption of no diffusion in the solid is also not always valid, as will be shown here for the Pb-Sn system. In these cases several investigators have proposed modifications to the nonequilibrium solidification equation (15,16). The amount of eutectic formed would be lowered by diffusion in the solid during freezing.

The objective of this investigation is to study macrosegregation by precise analytical determination of fraction eutectic and to compare the results with theoretical models previously presented (5-7, 15,16).

Nomenclature

$\overline{C}_\alpha$	average composition of dendrite
$\overline{C}_{\alpha\beta}$	average composition of two phase
C_E	eutectic composition
C_o	initial alloy composition
$\overline{C}_s$	average compositon of solid when $f_s = 1$
C_s	interface composition
ΔC_o	solute buildup for plane front, steady state: $C_o(1 - k)/k$
ΔT_o	undercooling at planar interface, steady state: $(T_L - T_S) = m_L \Delta C_o$
D_L	diffusion coefficient in liquid
f_α	fraction dendrite
$f_{\alpha\beta}$	fraction two phase
f_E	fraction eutectic
f_L	fraction liquid
f_s	fraction solid
G_L	thermal gradient in liquid, at tip
k	partition ratio, assumed constant
R	dendrite tip growth rate
s	Chalmers number, $D_L G_L / R\Delta T_o$

Experimental Procedures

Solidification Conditions

The General Purpose (Rocket) Furnace (GPF) located at the Marshall Space Flight Center (MSFC) was employed in these experiments. Several cylindrical ingots of Pb - 15 wt % Sn alloy, 1.6 cm in diameter and 6.3 cm high, were solidified in a nearly isothermal mode. The axial temperature gradient was maintained at less than 1.0 °C/cm. In addition, the samples were also slowly cooled in a controlled manner. Cooling rates typically were about 0.003 °C/sec. The cooling rate and temperature gradient were both nearly identical along the entire ingot throughout solidification, as shown in figure 2. In this figure curve number 1 gives the thermal profile for the top of the sample and curve number 6 gives the thermal profile for the bottom. Since the solidification rates and the temperature gradients are almost identical for the top and bottom of the sample, one would expect similar microstructures. As discussed later the dendrite arm spacings are very similar over the entire ingot. The cooling curve shown in Figure 2 reveals these solidification characteristics. The total solidification time is about 600 min. During solidification the mushy zone extense throughout the entire sample as indicated in figure 3. It is clear from this figure that final solidification occurs almost simultaneously throughout the sample and not in a fashion typical of directional solidification. The solidification behavior of our rather small samples is similar to that of large industrial ingots.

An automatic image analyzer was utilized in an attempt to obtain a fast and accurate technique for determining segregation. In using an image analyzer there are several variables which must be set to appropriate values. In the following section we will discuss these factors in some detail.

Analytical Measurements

A typical microstructure from a well polished and etched sample of our slow cooled Pb-15 wt % Sn alloy is illustrated in Figure 4. The dark phase is the lead-rich dendrite phase. The large patches of lighter areas, with a dark region within them, represent the two-phase tin-rich eutectic. Within the lead-rich dendrite we also see a finely distributed light etching phase. There are the tin-rich precipitates which formed when the alloy was cooled very slowly below the eutectic temperature. It is obvious that in order to obtain an accurate measure of the amount of eutectic in the sample, the contrast between the eutectic phase and the dendrite phase must be as high as possible.

The optical microstructure of the eteched sample with the optical image after the sample was allowed to tarnish is also shown in Figure 4. Tarnishing was accomplished by rinsing the polished, but unetched, sample with warm water. The Pb-rich phase is now darker, thus enhancing the contrast between the Pb-rich dendrite and the Sn-rich eutectic phase (17). Figure 4 also includes the "electronic" image of the tarnished sample as seen in the Quantimet. The "electronic" image may be seen to faithfully reproduce the optical image. The "electronic" image is obtained as follows.

The Quantimet converts the grey level at each picture point (pixel) in the image field into an electrical voltage. A pixel is the smallest resolvable area into which the image is divided for analysis. Each phase in the microstructure has its own characteristic grey level. If the grey levels for the various phases produce large enough differences in voltage, the differing signal from each pixel could be used for phase detection. The advantages of tarnishing the sample, or some other means of enhancing the phase contrast, should thus be obvious.

In addition to the sample preparation procedure described here, at least three other factors must be considered to determine the amount of eutectic accurately. These are the magnification of the image, the detect level, and amendments to the image (binary image), as discussed below.

(1) Magnification: The electronic image generated by the Quantimet at various magnifications is shown in Figure 5. The magnification must, clearly, be high enough to distinguish between the dendrite and eutectic phases but low enough to permit rapid analysis of the sample. Two large a magnification is undesirable because of the presence of tin-rich precipitates. At large magnifications the Quantimet would be unable to distinguish between the lighter tin-rich precipitates and the eutectic regions since both appear very light. At very low magnifications the Quantimet would view the lighter tin-rich precipitates as part of the (lighter) tin-rich eutectic. However, amend statements, described below, may be used to correct for the presence of tin-rich precipitates in the low-mag-electronic image. A magnification slightly less than 200x was used in our measurements. Several hundred measurements of eutectic fraction were thus obtained for each sample; the image field in the Quantimet corresponds to a sample area of ~450 by 600 μm.

(2) Detect Level (DL): The Quantimet 900 may be thought of as an electronic eye which is capable of detecting 64 shades of grey. An ideally black image is assigned a "detect level" of 1 and an ideal white image corresponds to a detect level of 64, with numbers between 1 and 64 indicating different levels of grey. The grey shading becomes lighter as the "detect level" increases. Note that the human eye can only detect 24 shades of grey (8).

The electronic images of the microstructure as depicted by the Quantimet in some of is different detection modes are shown in Figure 6. The electronic image of the Quantimet with all 64 detect levels turned on is illustrated in Figure 6. This is referred to as the "original" grey image. Also shown here are "binary" images used to quantify the fraction eutectic in the image field. The binary images are obtained as follows. The image seen at detect level 46 is the image obtained when all pixels which register a detect level >46 are assigned the ideal white level of 64, and those picels registering a detect level 46 and below are assigned the ideal black level of 1.

Note that the binary image at detect levels 40 and 44 still show some tin-rich precipitates whereas at detect levels greater than 46 some edges of the eutectic are beginning to appear dark and so will be left out of the measurement. A detect level of 46 was therefore used. We will discuss this point in more detail later.

(3) Amendment of the binary image: The measured eutectic fraction would be greater than the correct value if tin-rich precipitates, which appear lighter, are considered part of the eutectic. We must therefore amend the binary image, electronically. Amendment is a systematic two-step operation performed on the binary image, at a predetermined detect level, to produce a new binary image where in some features of the original image are first eroded and then subsequently dilated. During the erosion operation the Quantimet sweeps the edges of all detected features and removes one pixel at points every 45° apart. To complete the amendment cycle, the same number of pixels are added back to all surviving surfaces. If a particle disappears during any one cycle there will not be any corresponding adding of pixels. The erosion-dilation amend cycles can thus completely eliminate the tin-rich precipitate from the image, depending of course on the magnification and detect level.

In Figure 7 we illustrate how the binary image changes during the amend sequence. The bindary images in Figure 6 were obtained after performing appropriate amendments.

Finally, we discuss briefly a common source of error known as the offset error in image analysis of the kind used here. This error results from the fact that the video signal does not change sharply, Figure 8(a), but rather increases or decreases gradually as we cross the interphase boundary, Figure 8(b). The position of the feature boundary is usually taken to be the midpoint of the video signal ramp. This is the case in Figure 8(b), where the objective is to detect phase B but miss phase A. A detect level slightly below the midpoint of the video signal ramp, Figure 8(c), results in "shrinking" of phase B and an underestimate of the area fraction of phase B. However, the grey shading for the primary lead dendrites and the eutectic phase, in our case, are spaced far enough apart to allow the detect level to be set at the point where the eutectic edges corresponds to the midpoint of the signal. Error resulting from offsetting are thus expected to be quite small in our measurements.

Experimental Results

Figure 9 illustrates how the measured fraction eutectic at a given location in the sample varies with the detect level. At low detect levels, the measured fraction eutectic is quite large because the lighter Sn-rich precipitates are considered to be part of the eutectic. At high detect levels, the measured fraction eutectic begins to decrease because of filling in of portions of the eutectic particularly close to the boundary between Sn- and Pb-rich areas. In Figure 9 we indicate the Quantimet measurements for four adjacent image fields. In each case we find a plateau centered at about a detect level of 46. This detect level was used in most of our measurements. The plateau detect level was found to vary only slightly between various samples.

The error in our fraction eutectic measurements is thus closely related to how flat the percent eutectic versus detect level curve is, at the chosen DL, and is less than 0.2 percent of our quoted values.

The fraction eutectic versus distance from the bottom of the ingot are plotted in Figure 10. The large open circles are an average of some 400 measurements made in a transverse semicircular cross section. The solid dots are the average values from about 60 measurements at various radial locations (at a fixed height from the ingot bottom). It is interesting to note that both sets of measurements indicate the same trend: the fraction eutectic gradually increases from the bottom to the top of the ingot. This suggests an enrichment of the remaining liquid with tin and a gradual floating of the lighter tin-rich liquid to the top of the ingot.

This is confirmed by independent measurements of the variation of Sn content, Figure 11. Tin content was determined by conventional wet chemistry (Atomic Adsorption) and also from area rasters in an electron microprobe. This trend of increasing Sn from bottom to top compares quite well with the "averaged" longitudinal fraction eutectic profile obtained from the detailed variation shown in Figure 10. In order to make the comparison more clear between increasing tin content and increasing eutectic the detailed fraction eutectic profile is replotted in figure 11 as a more general average fraction eutectic curve.

DISCUSSION

Comparison of Fraction Eutectic Measurements with Theoretical Predictions

Since solidification was nearly isothermal, Equation (3), rather than Equation (1), may be used as a good starting point to estimate the amount of eutectic formed at the end of freezing. Both Equations (1) and (3), however, assume the partition ratio to be a constant throughout solidification, no diffusion in the solid and no undercooling prior to nucleation of the eutectic.

For the Pb - 15 wt % Sn alloy, k varies from about 0.5 close to the liquidus to 0.31 at the eutectic temperature. This means that in the early stages of solidification, relatively more tin will be incorporated into the dendrite than at the later stages. If we take k to be a constant, and equal to the lower value of 0.31 (commonly assumed for Pb-rich alloys), we would expect the amount of eutectic predicted to be higher than if we assumed k = 0.5. Values of f_E obtained in this manner for Equation (3) with k = 0.31 and 0.5 are 12.8 and 5.9 percent respectively. These values are represented by two of the four horizontal lines in Figure 12. Percent eutectic here is indicated by horizontal lines because Equation (3) or (1) do not predict any spatial variation. The average percent eutectic values reported in Figure 9 are replotted and are quite close to the estimated value taking k = 0.5. Inspite of this remarkable agreement, this is admittedly an oversimplified explanation for the experimentally observed behavior depicted in Figure 10.

We can allow k to vary as a function of C but now we must use the differential form of Equation (3),

$$df_L/f_L = dC_L/(k - 1)C_L \qquad (8)$$

Integrating numerically yields a value of $f_E = 0.088$. This is also indicated by a horizontal line in Figure 11. A total of 107 temperature intervals were considered, with k and C_L being obtained from the phase diagram for each interval. Equal temperature intervals of 1 °C were used.

Back-diffusion of the rejected solute into the solid during freezing will also result in a reduction of the amount of eutectic. The value of the dimensionless parameter α ($=D_s t_f/\lambda_s^2$), defined by Brody and Flemings (15), or α' ($=\alpha(1-\exp(-1/\alpha))-0.5\exp(-0.5\alpha)$) defined by Clyne and Kurz (16), is an indication of the importance of back-diffusion. We also performed a numerical integration where we simultaneously allowed for; (1) varying k with temperature and composition, (2) varying diffusion coefficient with temperature, and (3) varying dendrite arm spacing. The variation of secondary dendrite arm spacing, λ_s, as a function of temperature was obtained from a series of quench tests Figure 13. From the various samples the difference between the dendrite arm spacing at the bottom and the top was found to be statistically the same. Approximately a hundred dendrite arm spacings were measured for each sample. The diffusivity of Sn for the 15 wt % alloy was taken to be given by the Arrhenius equation, ($D_s = D_o\exp(-Q/RT)$), with $D_o = 0.16$ cm^2/sec and $Q = 21.3$ kcal/mole K. These values were estimated from values reported in the literature for dilute alloys (20). The local solidification time was extracted from the cooling curve shown in Figure 2. Thus, the three variables required to calculate the α parameter were all described as a function of temperature. A short computer program was write to allow for the continuous variation of these three terms. In this calculation we used the differential form of the parabolic model proposed by Brody and Flemings (B-F model), instead of Equation (8) α (or α') were thus allowed to change throughout solidification. In the early stages of solidification the diffusion coefficient is at a maximum and the secondary

arm spacing is at a minimum thus yielding a maximum in the α parameter. In other words back diffusion is largest at the beginning of solidification. In this study α was found to vary from 0.30 at the onset of solidification to 0.003 at the completion. (The differential form of the B-F model as well as other models proposed for solute redistribution have been summarized in ref. 19.)

Undercooling of the residual interdendritic liquid prior to eutectic solidification will also reduce the amount of eutectic (21). The calculations described above do not allow for this effect. In this study, the observed undercooling prior to eutectic solidification was found to be ~3.5 °C. With such a small eutectic undercooling one would expect negligibly small contributions to the reduction of eutectic.

Possible Sources of Error in Fraction Eutectic Measurements

When the interdendritic liquid is enriched to the eutectic composition, the only barrier to eutectic growth, in the Pb - 15 wt % Sn alloy, is the nucleation of the Sn-rich phase. Several investigators have suggested that Pb nucleates Sn (22-24). In a Pb - 30 wt % Sn alloy, the Sn-rich (β) phase nucleated at an undercooling of about 34 °C below the equilibrium β-liquidus, that is about 26 °C below the eutectic temperature, whereas in a Pb - 12.5 wt % Sn alloy, the (interdendritic) undercooling required for β nucleation is about 20 °C below the eutectic (25). Hence, we would expect interdendritic-eutectic solidification to begin by growth of the Sn-rich phase on the surface of the Pb-rich dendrites. The Sn-rich layer (Sn "halo") would then clearly mark the boundary between the dendrite and the eutectic phases (26). Other possible scenarios for nucleation and growth of the Pb - Sn eutectic are illustrated in Figure 14. A Pb-rich eutectic layer (Pb "halo") on the surface of the Pb dendrite can be imagined if the Sn-rich phase nucleates in the (undercooled) interdendritic liquid. It is difficult to imagime a Pb "halo" resulting from initiation of eutectic solidification by formation of a Pb-rich layer on the dendrite surface. The Pb "halos," if any, would be difficult to distinguish from the Pb dendrite and would introduce some error of unknown magnitude. (An estimate of the thickness of the first, or last, Pb-rich eutectic layer may perhaps be obtained by measuring the volume fraction of the two phases within the eutectic. We have attempted such corrections and these do not appear to be important. There is also the uncertainty concerning the extent of eutectic undercooling in our experiment.)

Other scenarios suggested in Figure 14 would permit a fairly accurate determination of the eutectic/dendrite boundary because of the partial coverage of the Pb dendrite surface with Sn. The accuracy of the Quantimet measurements therefore depend on the mechanism of eutectic nucleation and growth, however, calculations have shown that the error resulting from the Pb "halo" would be small for our samples.

Comparison of Quantimet Measurements with those Obtained from Other Techniques

Finally, Table I compares the Quantimet measurement for a randomly chosen image field, with values obtained from other well established quantitative metallographic techniques. Similar results were found for many other image fields. There is relatively good agreement between the different methods. Moreover, the error involved in point counting and lineal fraction techniques are larger. These manual measurements are more operator subjective and the time required to obtain a good statistical average for the sample is obviously much greater.

Concluding Remarks

Area fraction eutectic as determined with the Quantimet 900 is shown to be a suitable means for measuring macrosegregation in slowly cooled Pb - 15 wt % Sn alloys. The eutectic profile shows the same trend as the composition profiles determined by chemical and microprobe analysis. Quantimet measurements have several advantages over both chemical and microprobe methods. The advantages of automatic image analysis are: (1) the analysis is nondestructive, (2) the measurements are less sensitive to sample relief effects, (3) the analysis is quick (~1/2 min/measurement).

The models presently available yield predictions which are in fair agreement with the experimental results obtained in this investigation. The major source of error appears to be the selection of the diffusion parameters for Pb - 15 wt % Sn. This problem arises from the extrapolation length required to obtain the diffusion parameters from the data available in the literature. To eliminate any question about this error, diffusion experiments on Pb - 15 wt % Sn alloy are being planned.

References

1. M.C. Flemings: Solidification Processing, 1974, McGraw-Hill, New York, pp. 82, 93-130.

2. R.M. Sharp and M.C. Flemings: Metall. Trans., 1973, vol.4, pp. 997-1001.

3. T.F. Bower, H.D. Brody, and M.C. Flemings: Trans. Met. Soc. AIME, 1966, vol.236, pp. 624-634.

4. V. Laxmanan: in Rapidly Solidified Alloys and Their Mechanical and Magnetic Properties, B.C. Giessen, D.E. Polk, and A. I. Taub, eds., Materials Research Society, Pittsburgh, 41-50.

5. G.H. Gulliver: J. Inst. Met., 1913, vol. 9, pp. 120-157.

6. E. Scheil: Z. Metallk., 1942, vol. 34, pp. 70-72.

7. W.P. Pfann: J. Met., 1952, vol. 4, or; Trans. Met. Soc. AIME, 1952, vol. 194, pp. 747-753.

8. R.K. Crouch, A.L. Fripp, W.J. Debnam, I.O. Clark, and F.M. Carlson: in Materials Processing in the Reduced Gravity Environment of Space, G.E. Rindone, ed., North-Holland, New York, 1982, pp. 611-618.

9. P. Magnin and W. Kurz: Acta Met., 1987, vol. 35, pp. 1119-1128.

10. V. Laxmanan: Processing and Properties of Structural Alloys by Rapid Solidification, ASM, Metals Park, OH, 1987.

11. M.C. Flemings and G.E. Nereo: Trans. Met. Soc. AIME, 1967, vol. 239, pp. 1449-1461.

12. M.C. Flemings, R. Mehrabian, and G.E. Nereo: Trans. Met. Soc. AIME, 1968, vol. 242, pp. 41-49.

13. M.C. Flemings and G.E. Nero: Trans. Met. Soc. AIME, 1968, vol. 242, pp. 50-55.

14. R. Mehrabian, M. Keane, and M.C. Flemings: Metall. Trans., 1970, vol. 1, pp. 1209-1220.

15. H.D. Brody and M.C. Flemings: Trans. Met. Soc. AIME, 1966, vol. 236, pp. 615-624.

16. T.W. Clyne and W. Kurz: Metall. Trans. A, 1981, vol. 12, pp. 965-971.

17. C. DiMartini: Metals Handbook, vol. 9, ASM, Metals Park, OH, 1985, pp. 415-424.

18. T. Henson and H. Henson: Metals Handbook, vol 9, ASM, Metals Park, OH, 1985, pp.152-154.

19. V. Laxmanan, A. Studer, L. Wang, J.F. Wallace and E.A. Winsa: NASA TM-89885, 1986.

20. J. Oberschmidt, K.K. Kim, and D. Gupta: J. Appl. Phys., 1982, vol. 53, pp. 5672-5677.

21. M.C. Flemings: in Metallurgical Treatises, J.K. Tien and J.F. Ellito, eds., AIME, Warrendale, PA, 1981, pp. 291-300.

22. J.H. Hollomon and D. Turnbull: J. Met., 1951, vol. 3, or; Trans. Met. Soc. AIME, 1951, vol. 191, pp. 803-805.

23. B.E. Sundquist and L.F. Mondolfo: Trans. Met. Soc. AIME, 1961, vol. 221, pp. 157-164.

24. W.V. Youdelis and S.P. Iyer: Met. Sci., 1975, vol. 9, pp. 289-290.

25. H.C. deGroh III and V. Laxmanan: these proceedings.

26. M.F.X. Gigliotti Jr, G.A. Colligan and G.L.F. Powell: Metall. Trans., 1970, vol. 1, pp. 891-897.

TABLE I. - COMPARISON OF QUANTITATIVE METALLOGRAPHY METHODS

Methods	Fraction eutectic	Comments
Quantimet	0.0867	Detect level = 46
Lineal fraction	.0916	1/4" line spacing
Point count	.0846	1/4x1/4" grid
Point count	.0872	1/20x1/20" grid

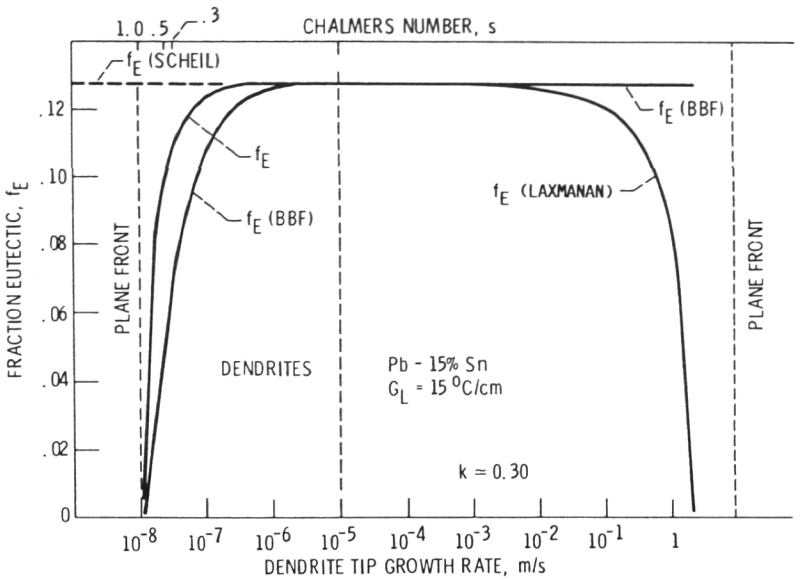

FIGURE 1. - FRACTION OF TWO-PHASE SOLID (EUTECTIC-LIKE) FORMED AT END OF SOLIDIFICATION. THESE CALCULATIONS ACCOUNT FOR THE FACT THAT THE TWO-PHASE SOLID ACTUALLY HAS A COMPOSITION LESS THAN C_E.

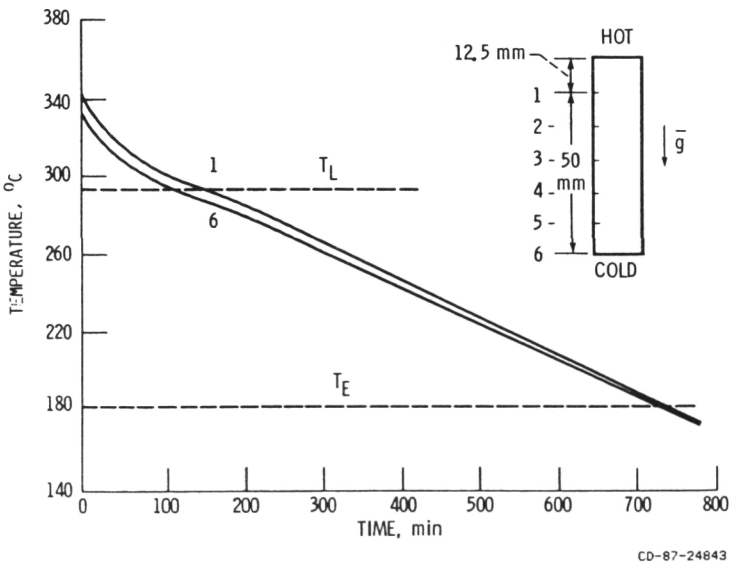

FIGURE 2. - TYPICAL TEMPERATURE-TIME PLOT FOR SLOWLY COOLED Pb-15 wt % Sn SAMPLE IN SINGLE-CAVITY GPF SIMULATOR.

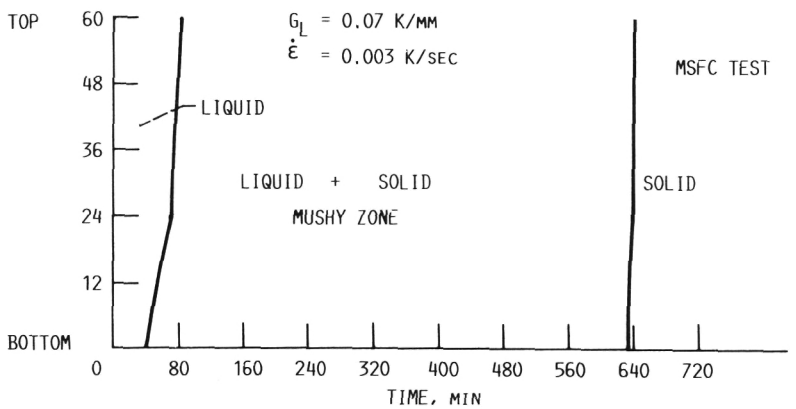

FIGURE 3. - COMPARISON OF EVOLUTION OF MUSHY ZONE (TWO-PHASE, LIQUID PLUS SOLID, REGION).

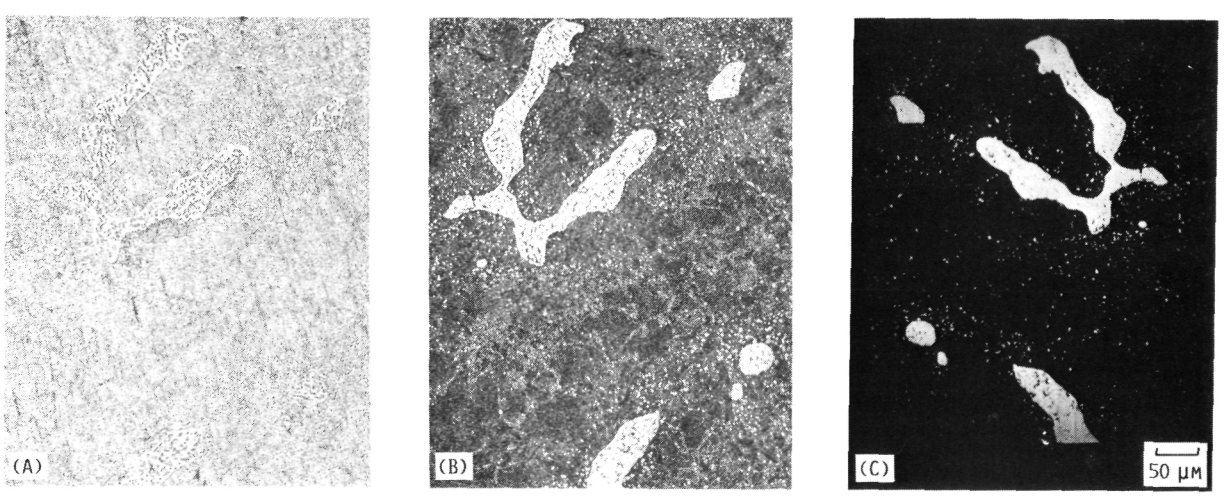

FIGURE 4. - TYPICAL MICROSTRUCTURE VIEWED UNDER VARIOUS CONDITIONS: (A) POLISHED AND ETCHED, (B) TARNISHED, AND (C) QUANTIMET'S ELECTRONIC IMAGE.

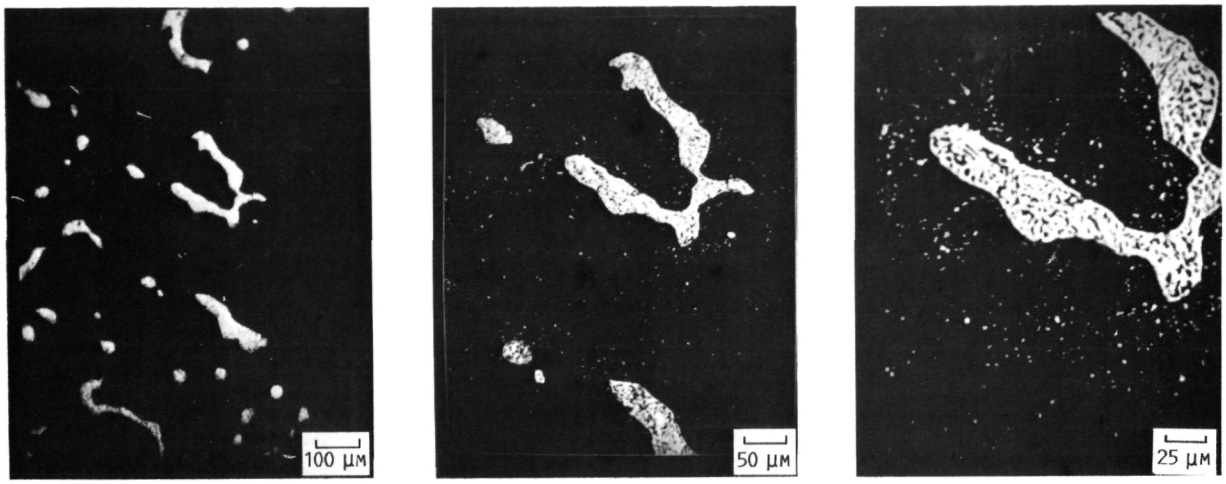

100 X 200 X 400 X

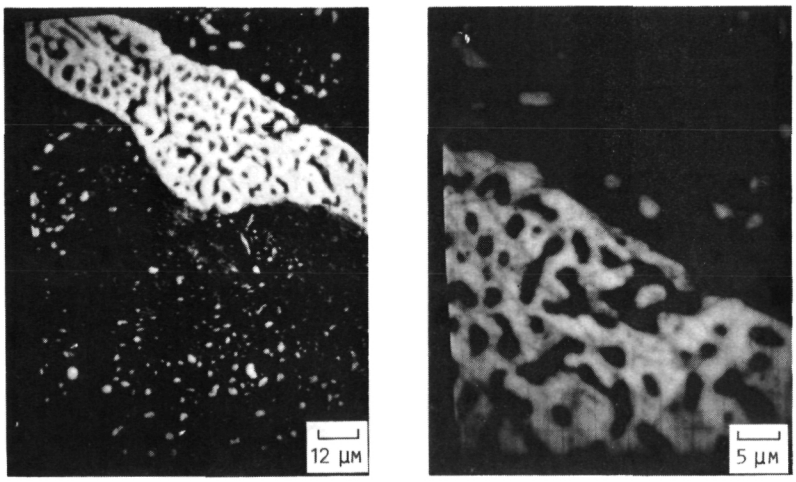

800 X 2000 X

FIGURE 5. - ELECTRONIC IMAGE SHOWING THE RANGE OF MAGNIFICATION AVAILABLE ON THE QUANTIMET, 200x WAS SELECTED.

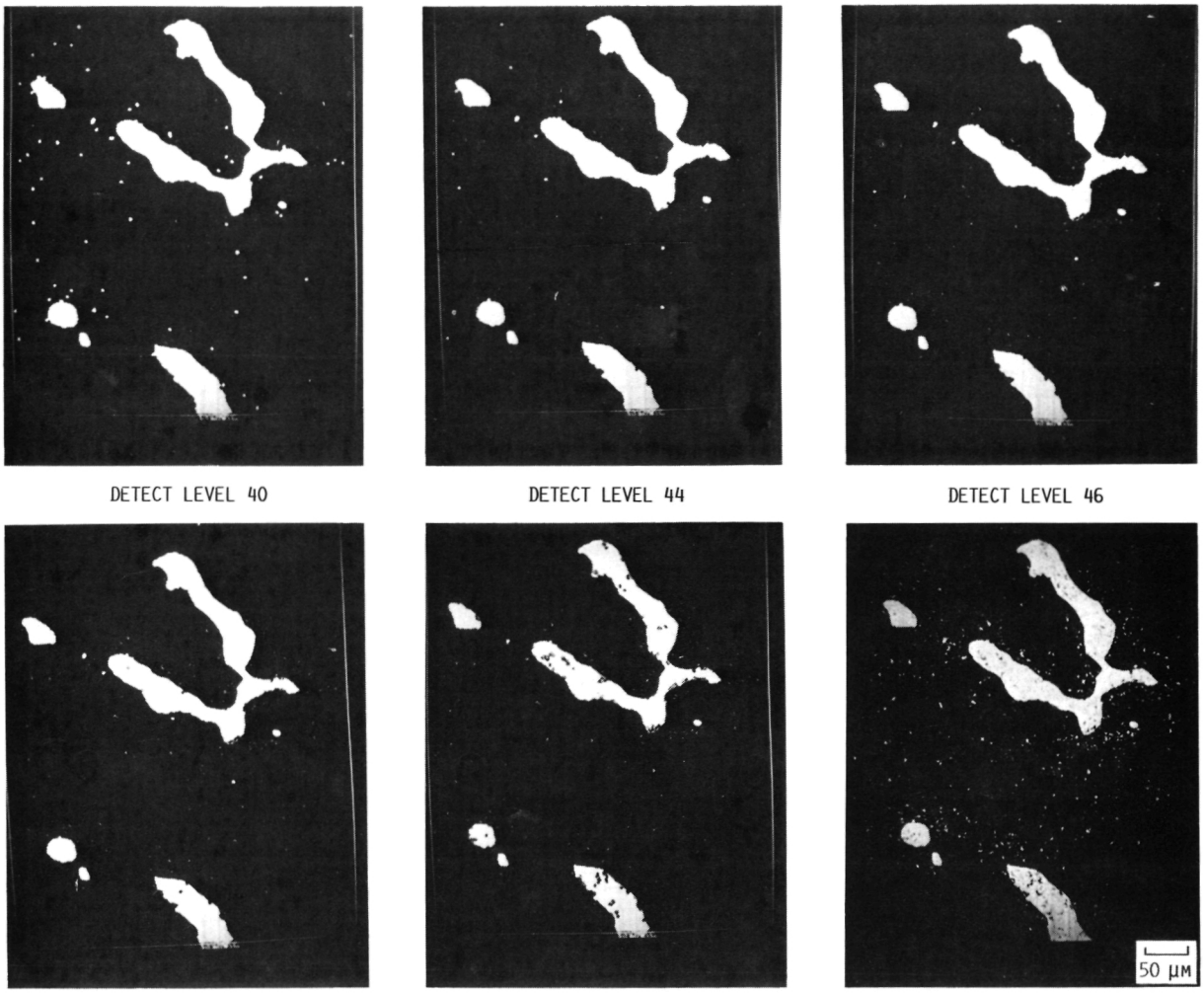

FIGURE 6. - SEVERAL IMAGES OBTAINED FOR VARIOUS DETECT LEVELS ON THE CAMBRIDGE QUANTIMET 900. CARE MUST BE TAKEN IN CHOOSING THE DETECT LEVEL TO AVOID BOTH OVERFILLING AND UNDERFILLING.

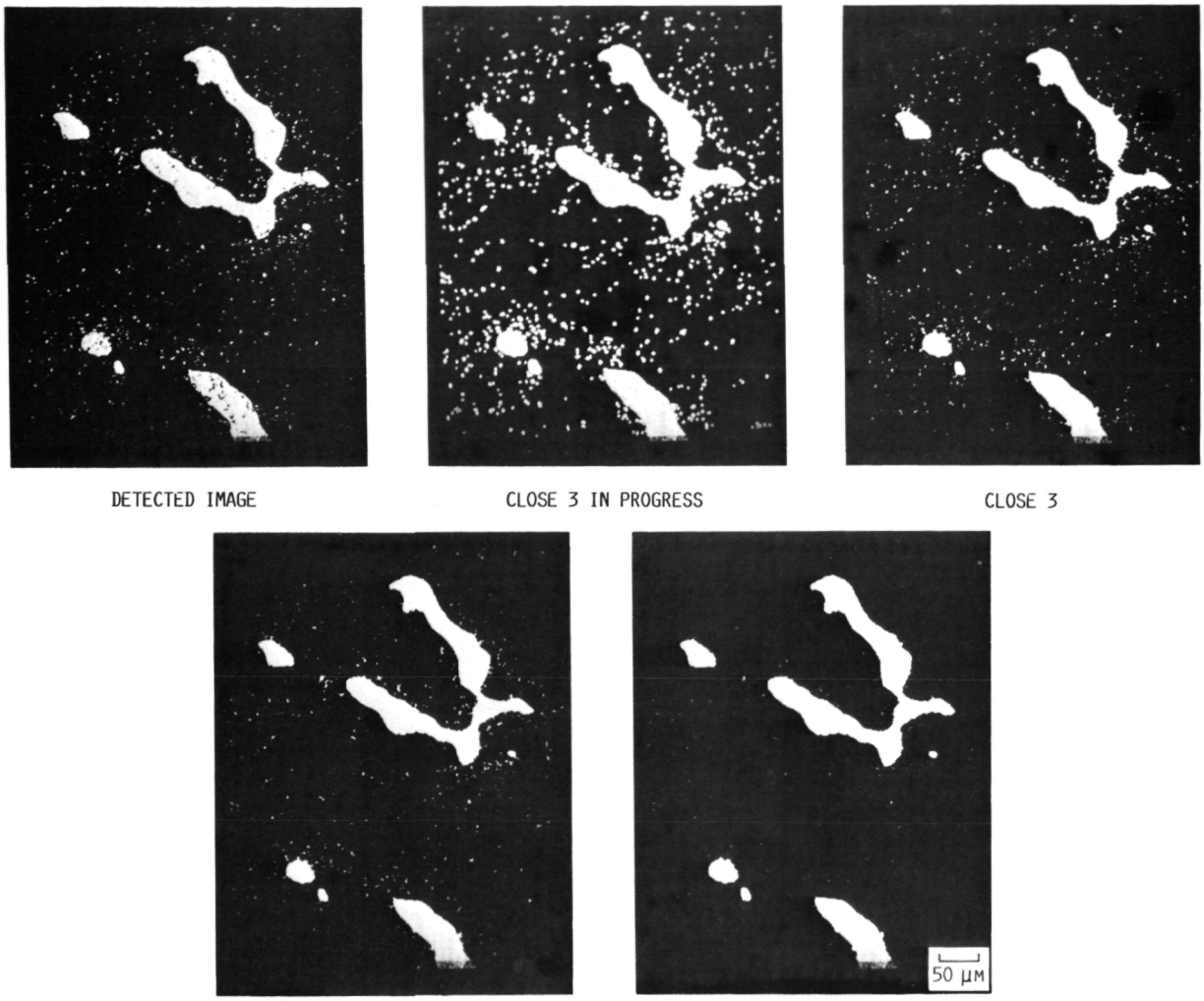

DETECTED IMAGE

CLOSE 3 IN PROGRESS

CLOSE 3

CLOSE 3 - OPEN 3 IN PROGRESS

CLOSE 3 - OPEN 3

FIGURE 7. - PICTORIAL SEQUENCE OF THE AMEND OPERATION.

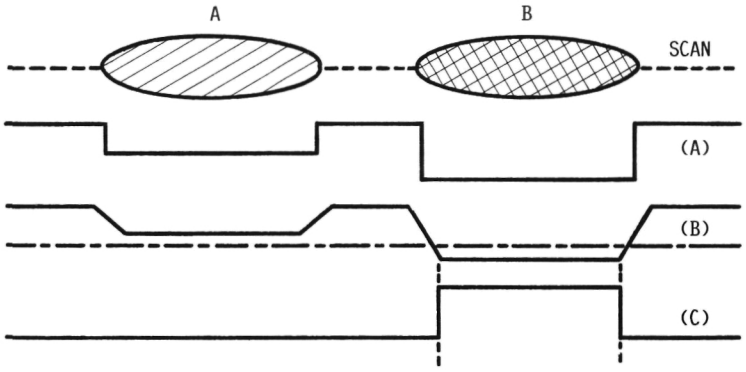

FIGURE 8. - POSSIBLE ERROR RESULTING FROM THE VIDEO SIGNAL. (A) IDEAL VIDEO SIGNAL. (B) PRACTICAL VIDEO SIGNAL WITH THE THRESHOLD SET TO DETECT B BUT AVOID A. (C) DETECTED OUTPUT SHRUNK ALL AROUND THE PERIMETER.

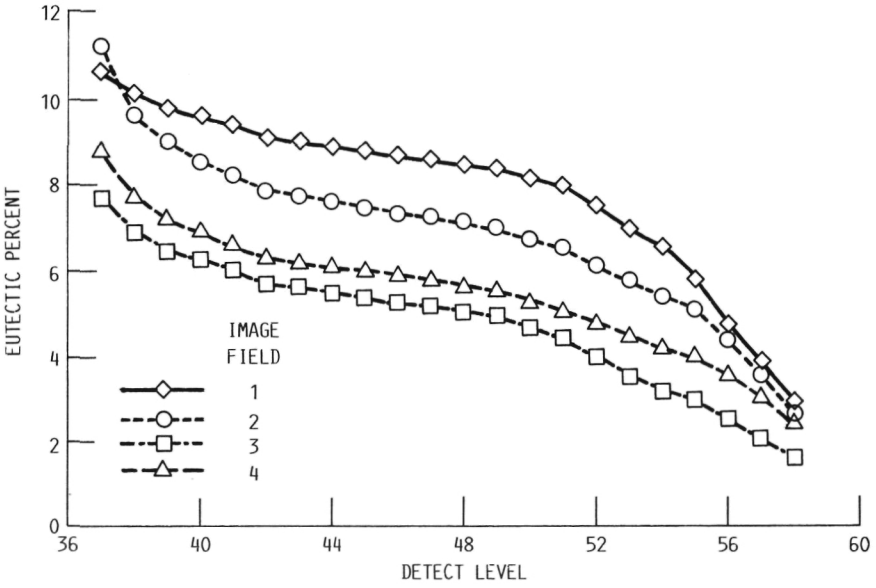

FIGURE 9. - AREA FRACTION EUTECTIC VERSUS DETECT LEVEL MEASURED ON A CAMBRIDGE QUANTIMET 900.

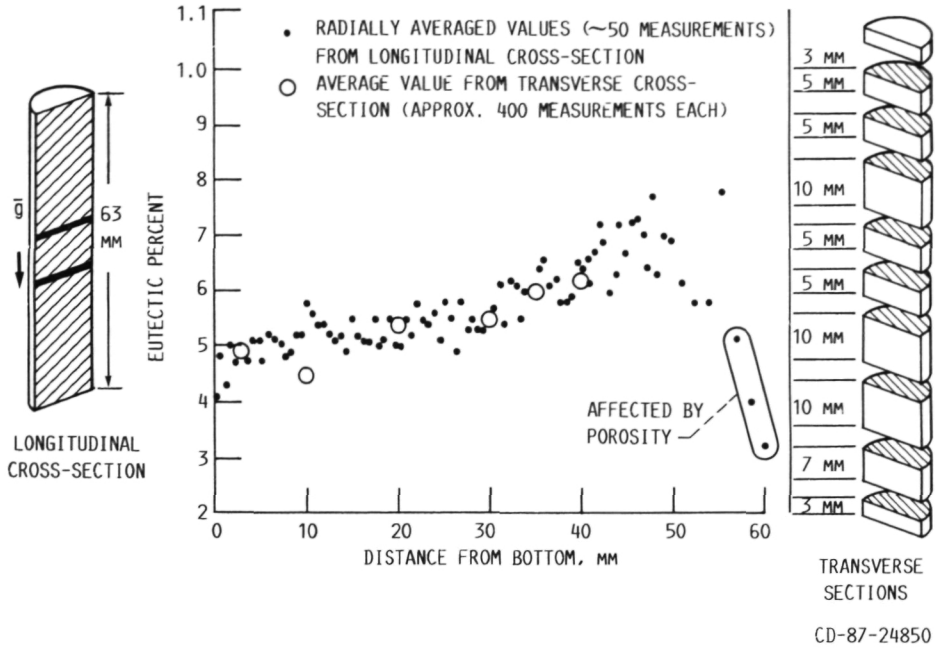

FIGURE 10. - PERCENT EUTECTIC VERSUS DISTANCE IN A SLOWLY COOLED Pn- 15 WT PERCENT Sn ALLOY.

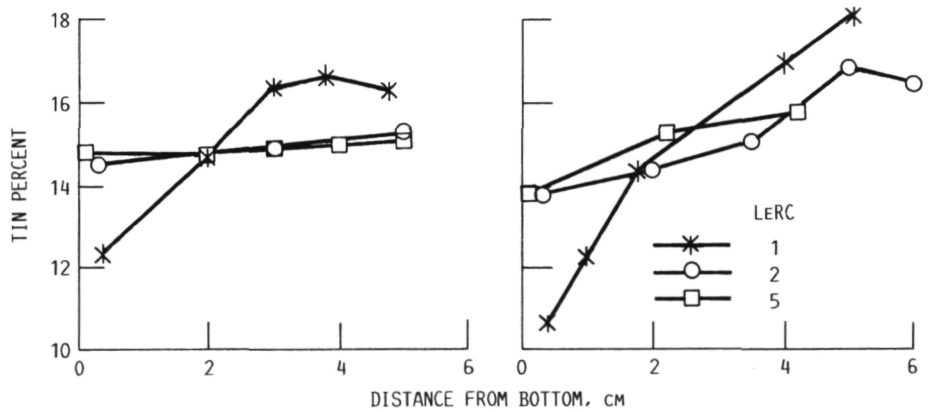

FIGURE 11. - TIN CONTENT VERSUS LONGITUDINAL DISTANCE FOR Pb- 15 WT PERCENT Sn ALLOYS. COMPOSITION DETERMINED BY: (A) ATOMIC ABSORPTION SPECTROMETRY AND (B) MICROPROBE ANALYSIS.

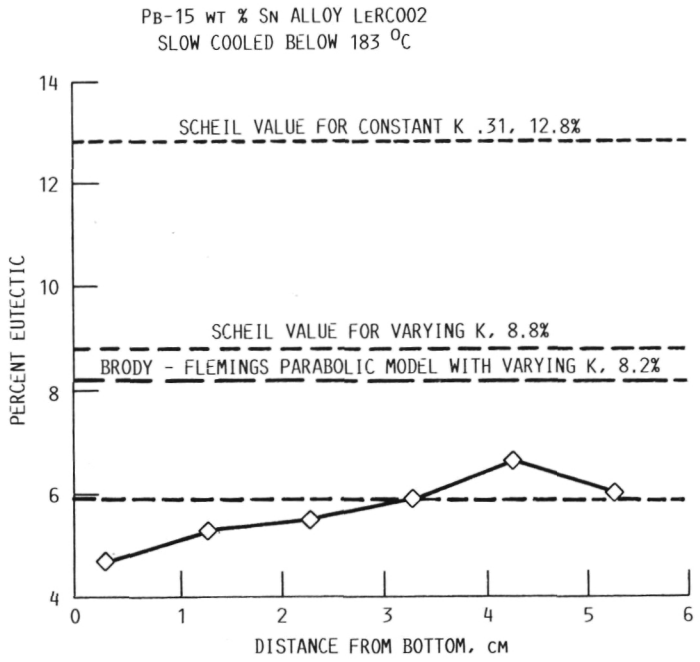

FIGURE 12. - PREDICTED PERCENT EUTECTIC OBTAINED FROM VARIOUS MODELS COMPARED WITH THE EXPERIMENTALLY MEASURED VALUES.

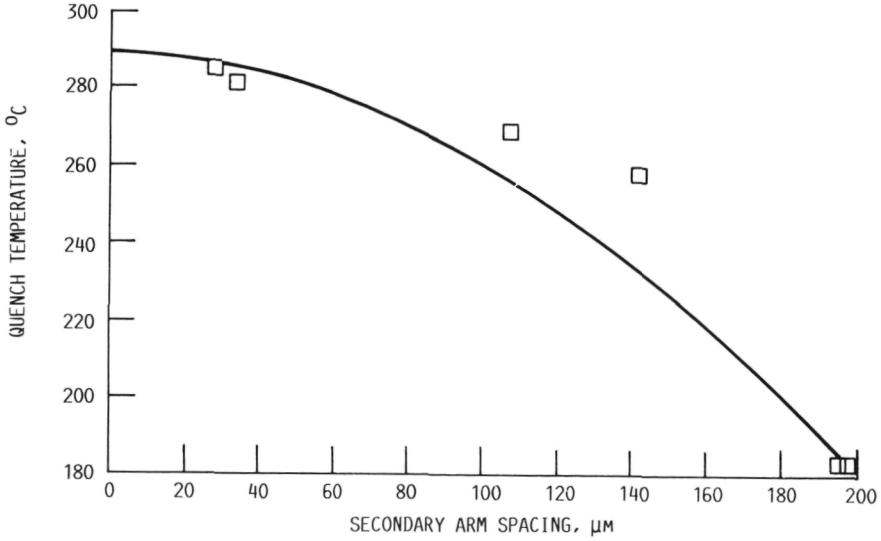

FIGURE 13. - SUMMARY OF SECONDARY DENDRITE ARM SPACING MEASUREMENTS IN "ISOTHERMALLY" PROCESSED SAMPLES.

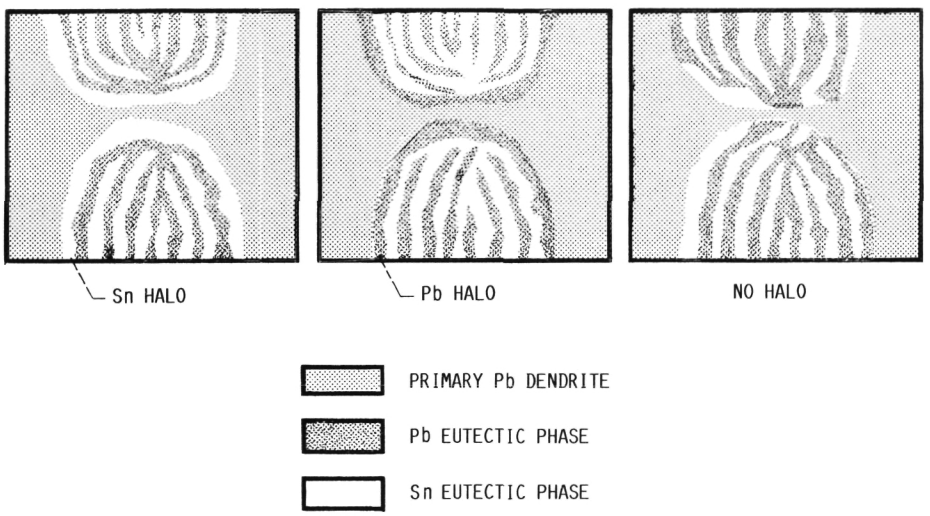

FIGURE 14. - POSSIBLE SCENARIOS FOR THE SOLIDIFICATION OF THE Pb-Sn EUTECTIC.

NASA
National Aeronautics and Space Administration

Report Documentation Page

1. Report No.	2. Government Accession No.	3. Recipient's Catalog No.
NASA CR-180830		

4. Title and Subtitle	5. Report Date
Fraction Eutectic Measurements in Slowly Cooled Pb - 15 wt % Sn Alloys	June 1988
	6. Performing Organization Code

7. Author(s)	8. Performing Organization Report No.
Anthony C. Studer and V. Laxmanan	None (E-3762)
	10. Work Unit No. 674-25-05

9. Performing Organization Name and Address	11. Contract or Grant No.
Case Western Reserve University Dept. of Materials Science and Engineering Cleveland, Ohio 44106	NCC 3-74
	13. Type of Report and Period Covered Contractor Report Final

12. Sponsoring Agency Name and Address	14. Sponsoring Agency Code
National Aeronautics and Space Administration Washington, D.C. 44135-3191	

15. Supplementary Notes

Project Manager, Hugh R. Gray, Materials Division, NASA Lewis Research Center. Prepared for the 1987 Fall Meeting of The Metallurgical Society, Cincinnati, Ohio, October 12-14, 1987.

16. Abstract

A space shuttle experiment employing the General Purpose Furnace (GPF) in its isothermal mode of operation is currently manifested for flight circa 1989. The central aim of this experiment is to investigate the role of gravity in a slowly, and isothermally, cooled sample (cooling rates about 0.003 K/sec, thermal gradients <0.05 K/mm, the top slightly hotter than the bottom) of a binary Pb - 15 wt % Sn alloy. Ground-based work in support of the microgravity experiment will be discussed. In particular, it will be shown that fraction eutectic measurements using an image analyzer, can be used to satisfactorily describe macrosegregation occurring in these slowly cooled ingots.

17. Key Words (Suggested by Author(s))	18. Distribution Statement
Eutectic; Lead-tin alloys; Isothermal; Dendritic; Macrosegregation	Unclassified - Unlimited Subject Category 26

19. Security Classif. (of this report)	20. Security Classif. (of this page)	21. No of pages	22. Price*
Unclassified	Unclassified	20	A02

NASA FORM 1626 OCT 86

*For sale by the National Technical Information Service, Springfield, Virginia 22161